

Microwave Optomechanically Induced Transparency and Absorption Between 250 and 450 mK

Sumit Kumar · Dylan Cattiaux · Eddy Collin · Andrew Fefferman · Xin Zhou

February 1, 2022

Abstract High-quality microwave amplifiers and notch-filters can be made from microwave optomechanical systems in which a mechanical resonator is coupled to a microwave cavity by radiation pressure. These amplifiers and filters rely on optomechanically induced transparency (OMIT) and absorption (OMIA), respectively. Such devices can amplify microwave signals with large, controllable gain, high dynamic range and very low noise. Furthermore, extremely narrowband filters can be constructed with this technique. We briefly review previous measurements of microwave OMIT and OMIA before reporting our own measurements of these phenomena, which cover a larger parameter space than has been explored in previous works. In particular, we vary probe frequency, pump frequency, pumping scheme (red or blue), probe power, pump power and temperature. We find excellent agreement between our measurements and the predictions of input/output theory, thereby guiding further development of microwave devices based on nanomechanics.

1 Introduction

Superconducting microwave circuits have had a strong impact on science and technology in recent years. Initial experiments in circuit cavity quantum electrodynamics [1,2] have led to massive efforts in the field of quantum information processing with superconducting qubits [3]. Superconducting circuits are also used as highly sensitive astrophysical detectors [4]. At the same time, coupling mechanical and electromagnetic degrees of freedom via radiation pressure

Sumit Kumar · Dylan Cattiaux · Eddy Collin · Andrew Fefferman
Université Grenoble Alpes and Institut Néel, CNRS, Grenoble, France
E-mail: andrew.fefferman@neel.cnrs.fr

Xin Zhou
Univ. Lille, CNRS, UMR 8520 - IEMN, Lille, France

has led to a plethora of fascinating results. Initially light at (nearly) visible wavelengths was employed for these optomechanical studies [5, 6, 7, 8, 9].

More recently, the techniques of superconducting microwave circuits and optomechanics were combined by shifting from visible light to microwave frequencies [10]. This was followed by impressive achievements in areas including quantum control of mechanical resonators [11] as well as microwave circulators [12, 13] and amplifiers [14].

Microwave amplifiers and notch filters can rely on optomechanically induced transparency (OMIT) and absorption (OMIA), respectively. These phenomena are observed when a strong pump and a weak probe with a frequency difference near the mechanical resonance frequency are simultaneously applied to the electromagnetic resonator, resulting in a change in the transmission of the probe. Several workers have reported measurements of OMIT and OMIA. Weis *et al.* [15] observed OMIT in toroidal whispering-gallery-mode microresonators illuminated by a laser operating at a wavelength of 775 nm. In this work the dependence of the probe transmission on pump power and detuning was investigated. Safavi-Naeini *et al.* [16] observed OMIT and OMIA in optomechanical crystals illuminated by laser light with wavelength of 1550 nm. Here the pump power and detuning was varied, and measurements were made at 8.7 kelvin and at room temperature.

In one of the first demonstrations of OMIT at microwave frequencies, Teufel *et al.* [17] presented highly sensitive measurements of the probe transmission upon varying the pump power and detuning. Shortly thereafter, an analysis of the use of OMIT for microwave amplification, as well as the observation of OMIA at microwave frequencies, was presented by Massel *et al.* [14]. In that work, the dependence of the probe transmission on pump power was studied. Hocke *et al.* focused on microwave OMIA and reported transmission as a function of detuning and drive power up to the mechanical parametric instability [18]. Zhou *et al.* returned to microwave OMIT and scanned the probe power, thereby driving the mechanical resonator strongly enough so that its Duffing non-linearity became significant [19]. The ability of microwave optomechanical amplifiers to function at high probe power was later confirmed with a relatively elaborate device [20]. Recent work has demonstrated the advantage of combining mechanical parametric amplification with OMIT [21] as well as microwave amplification in the absence of the dynamical backaction responsible for amplification of mechanical motion [22]. The lack of dynamical backaction has the advantage that quantum-limited microwave amplification could be achieved even in the presence of large thermal occupation of the mechanical mode [22].

Here we report the results of our two tone measurements of a microwave optomechanical device, in which we explore a larger parameter space than has been covered in previous works. In particular, we vary probe frequency, pump frequency, pumping scheme (red or blue), probe power, pump power and temperature. We demonstrate that the theoretical transmission derived from input/output theory is in excellent agreement with our measurements over the entire parameter range.

2 Optomechanically induced transparency and absorption

OMIT and OMIA can be observed in systems where a mechanical resonator is coupled to an electromagnetic resonator (the cavity) in such a way that the motion of the former changes the resonance frequency of the latter. The interaction between a single phonon and a single photon is characterized by g_0 , the vacuum optomechanical coupling strength, which is the frequency shift of the cavity due to zero point motion of the mechanical resonator. When the cavity is driven by a pump at frequency ω_d and a probe at frequency ω_p (Fig. 1a), there is a component of the resulting radiation pressure force at the difference frequency $\Omega = \omega_p - \omega_d$. We denote the mechanical resonance frequency by Ω_m . When $||\Omega| - \Omega_m|$ is less than or approximately equal to the mechanical linewidth, the response of the mechanical element is appreciable. Now its motion yields up-conversion or down-conversion of the photons by an amount $|\Omega|$, yielding sidebands in the microwave spectrum. One of the two sidebands of the pump is at a frequency that coincides with the probe frequency. Whether this is the upper or lower sideband depends on the sign of Ω . The probe and the coincident sideband interfere constructively or destructively depending on their relative phases, resulting in a change in the transmission of the probe relative to the value it would have in the absence of optomechanical coupling. This effect is most significant when the probe frequency is within about one half linewidth κ of the cavity resonance frequency ω_c . This is equivalent to $|\Delta + \Omega| < \approx \kappa/2$, where we define $\Delta = \omega_d - \omega_c$.

The magnitude of the response of the mechanical resonator to the radiation pressure at the beat frequency Ω influences the probe transmission. The mechanical response depends not only on the difference between the driving frequency and the mechanical resonance $|\Omega| - \Omega_m$ and the intrinsic linewidth of the mechanical resonator Γ_m but also on dynamical backaction due to the pump [23]. The backaction yields an effective mechanical linewidth Γ_{eff} , which is greater than Γ_m for $\omega_c - \omega_d \approx \Omega_m$ (“red pumping”) and less than Γ_m for $\omega_d - \omega_c \approx \Omega_m$ (“blue pumping”).

The theoretical probe transmission S_{21} in the presence of a pump, consistent with the qualitative discussion of OMIT and OMIA above, has been derived in previous works [24, 19]. The output from the microwave cavity \hat{a}_{out} is related to the applied field \hat{a}_{in} by [25]

$$\hat{a}_{out} = \hat{a}_{in} + \sqrt{\kappa_{ext}/2} \hat{a}$$

where κ_{ext} is the part of the cavity linewidth due to coupling to the feedline and \hat{a} is the cavity field. This input/output relation, along with the equations of motion for the microwave cavity field [26] and the mechanical oscillator position x , is the starting point for the derivation of the probe S_{21} [19]. We define the respective cavity and mechanical susceptibilities as $\chi_c^{-1}(\omega) = \kappa/2 - i(\omega - \omega_c)$ and $\chi_m^{-1}(\omega) = \Gamma_m/2 - i(\omega - \omega_d \pm \Omega_m)$ where the upper (lower) sign is for blue (red) pumping. Then

$$S_{21}(\omega_p) = 1 - \frac{\chi_c(\omega_p) \kappa_{ext}/2}{1 \mp g_0^2 n_{cav} \chi_c(\omega_p) \chi_m(\omega_p)} \quad (1)$$

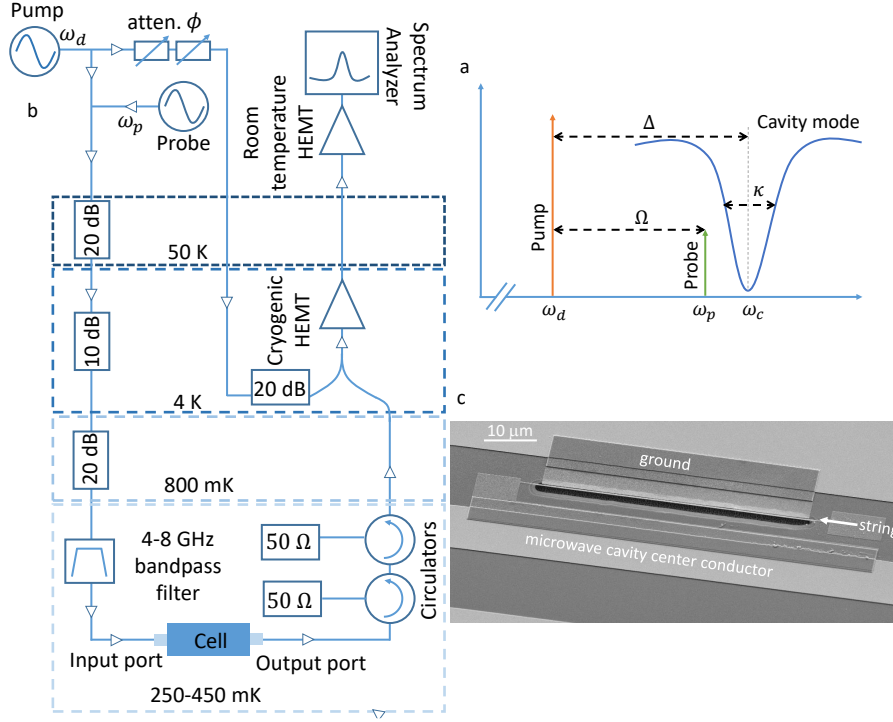


Fig. 1 (a) The pump and probe scheme, (b) the microwave circuit and (c) the nanomechanical resonator, which is coupled to the microwave cavity.

where

$$\begin{aligned}\chi_c^{-1}(\omega_p) &= \frac{\kappa}{2} - i(\Omega + \Delta), \\ \chi_m^{-1}(\omega_p) &= \frac{\Gamma_m}{2} - i(\Omega \pm \Omega_m),\end{aligned}$$

and

$$n_{cav} = \frac{P_{in}\kappa_{ext}}{2\hbar\omega_d} |\chi_c(\omega_d)|^2. \quad (2)$$

Here κ_{ext} is the part of the cavity linewidth due to intentional coupling to the feedline, n_{cav} is the number of photons stored in the cavity due to the pump, and P_{in} is the pump power at the input of the optomechanical device.

3 Experiment

Our optomechanical device and microwave measurement circuit are similar to ones used in previous works, e.g., [10, 27]. A circuit diagram is shown in Fig. 1b. The pump and probe tones are combined at room temperature. These signals then pass through attenuators, which decrease the thermal noise level, and a bandpass filter before reaching the input port of the experimental cell. The

bandpass filter is used to remove spurious signals coming from, e.g., the microwave generators. The transmitted signal that exits the cell passes through two circulators, which prevent noise traveling down the detection line from entering the output port of the cell. At the 4 kelvin plate, the pump signal that was transmitted through the cell is canceled to avoid saturating the amplifiers. The resulting signal passes through a cryogenic high electron mobility transistor (HEMT) amplifier and a room temperature HEMT amplifier before measurement with a spectrum analyzer.

The experimental cell is a box made of annealed CuC2. It is pressed against the mixing chamber plate of the cryogen-free dilution refrigerator. Inside the cell the input and output coaxial transmission lines are soldered to gold coplanar waveguides (CPW) on a circuit board, which are in turn microbonded to the ends of a niobium CPW on a chip. The chip is made of silicon and is coated with 100 nm of high stress silicon nitride. A $\lambda/4$ CPW resonator is also present on the chip and forms a cavity with resonance frequency $\omega_c/2\pi = 6$ GHz. The open end of the $\lambda/4$ resonator is precisely situated relative to the CPW feedline to achieve the desired coupling. The strength of the coupling is characterized by an external cavity linewidth $\kappa_{ext}/2\pi = 44$ kHz. The total cavity linewidth is $\kappa/2\pi \approx 100$ kHz, so that the condition for critical coupling $\kappa = 2\kappa_{ext}$ is nearly satisfied.

The mechanical element is a vibrating string made from silicon nitride at the open end of the cavity (Fig. 1c). Its geometry was defined by a 30 nm thick aluminum layer that served as a reactive ion etch (RIE) mask. After the anisotropic RIE, the string was released by selective XeF_2 etching of the silicon substrate. The aluminum was not removed after etching, and it yields electrostatic coupling between the vibrating string and the cavity characterized by the coupling strength $g_0/2\pi = 0.56$ Hz. The string has a length of $50 \mu\text{m}$ and a resonance frequency $\Omega_m/2\pi = 3.8$ MHz.

4 Results and Discussion

The measurements were carried out at sample temperatures of 250, 350 and 450 mK. For each temperature, pump power and probe power setting, the pump and probe frequencies were scanned and the probe transmission was measured. Figure 2 shows our measurements at 250 mK with red pumping yielding $n_{cav} = 1.3 \times 10^6$ and a probe power of -116 dBm at the input of the cell. The transmission measurements were made by setting ω_d and sweeping the probe frequency ω_p over a narrow range around $\omega_d + \Omega_m$ for red pumping and around $\omega_d - \Omega_m$ for blue pumping. The width of the probe frequency sweeps was comparable to the mechanical linewidth, so that it encompassed the OMIT/OMIA resonance. These measurements were made at a range of pump frequencies ω_d such that the set of center frequencies of the narrow probe frequency sweeps spanned the microwave resonance. These narrow sweeps appear as vertical lines on the scale of the main panel of Fig. 2; two of the sweeps are enlarged in the insets.

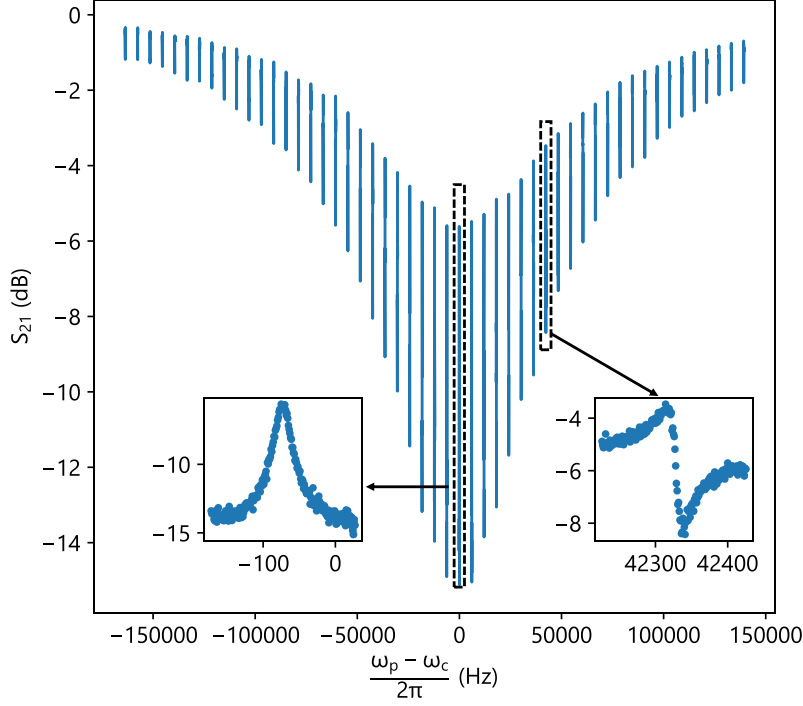


Fig. 2 Probe transmission measurements at 250 mK with red pumping yielding $n_{cav} = 1.3 \times 10^6$ and a probe power of -116 dBm at the input of the cell. The narrow probe frequency sweeps appear as vertical lines. The insets show enlargements of the indicated sweeps.

Figure 3 shows OMIT at the microwave resonance. Any residual detuning is very small compared with the cavity linewidth. These data were acquired under red pumping ($\omega_d = \omega_c - \Omega_m$), and the dependence on temperature, probe power and pump power is shown. The intracavity pump photon numbers and probe powers at the input of the cavity are based on a careful measurement of the attenuation of the transmission line connecting the generator to the microwave cavity. At constant temperature and probe power the amplitude of the OMIT resonance increases with pump power because (1) the mechanical mode is driven more strongly and (2) more pump photons are available for up-conversion to the probe frequency by interaction with the mechanical mode. The resulting upper sideband interferes constructively with the probe. The width of the OMIT resonance increases with pump power due to dynamical backaction on the mechanical mode. The curves represent fits of the theoretical $|S_{21}|$ (Eq. 1) to the data. Single values of Ω_m and Γ_m were chosen for each temperature to optimize the fits of the theoretical transmission to the entirety

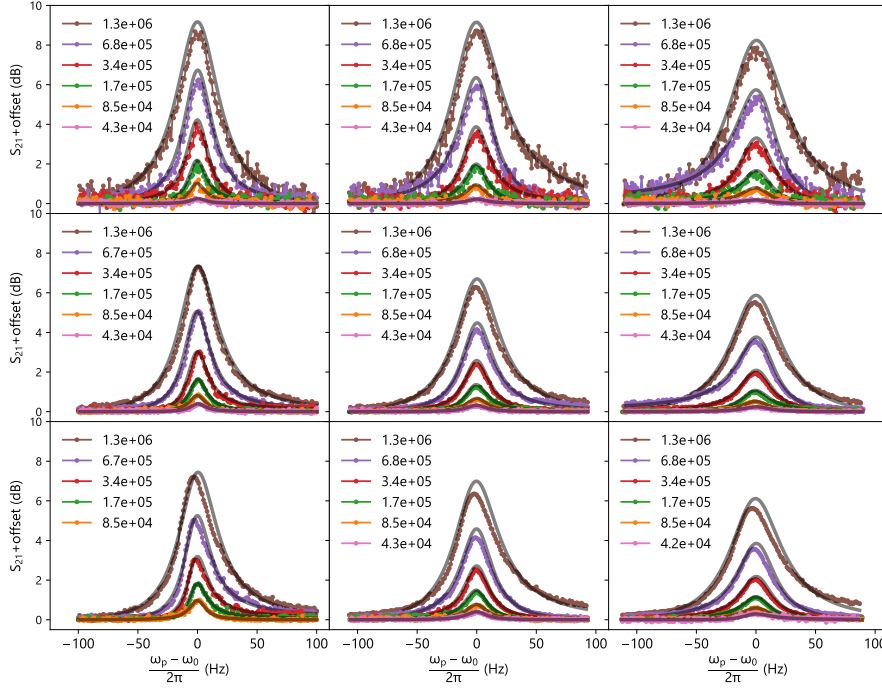


Fig. 3 Main panel: Probe transmission measurements at the indicated temperatures and probe powers referenced to the input of the cavity. Red pumping was applied, yielding the specified intracavity pump photon numbers. The transmission curves are offset vertically for clarity and ω_0 is an offset close to ω_c . Grey curves are fits of Eq. 1 to the data.

of our measurements of this device. At 350 (450) mK, $\Omega_m/2\pi$ is higher than its 250 mK value by 7 (12) Hz. The intrinsic mechanical linewidths $\Gamma_m/2\pi$ at 250, 350 and 450 mK are 15.3, 20.0 and 26.8 Hz, respectively. The values of ω_c and κ were allowed to vary to account for the dependence of these parameters on cavity temperature and photon population. The dependence of κ on probe power is primarily responsible for the dependence of the transmission on probe power shown in Fig. 3.

Figure 4 shows OMIA on the microwave resonance at the same probe powers and temperatures as in Fig. 3. These data were acquired under blue pumping ($\omega_d = \omega_c + \Omega_m$). As for red pumping, the driving force acting on the string and the number of pump photons stored in the cavity increase with pump power. But for blue pumping the lower sideband interferes destructively with the probe, yielding decreased transmission of the probe in Fig. 4. Furthermore, the width of the optomechanical resonance decreases with pump power due to dynamical backaction on the mechanical mode. At pump powers that are higher than those shown in Fig. 4, Γ_{eff} vanishes and the mechanical mode undergoes self-sustained oscillations. As we approach the auto-oscillation

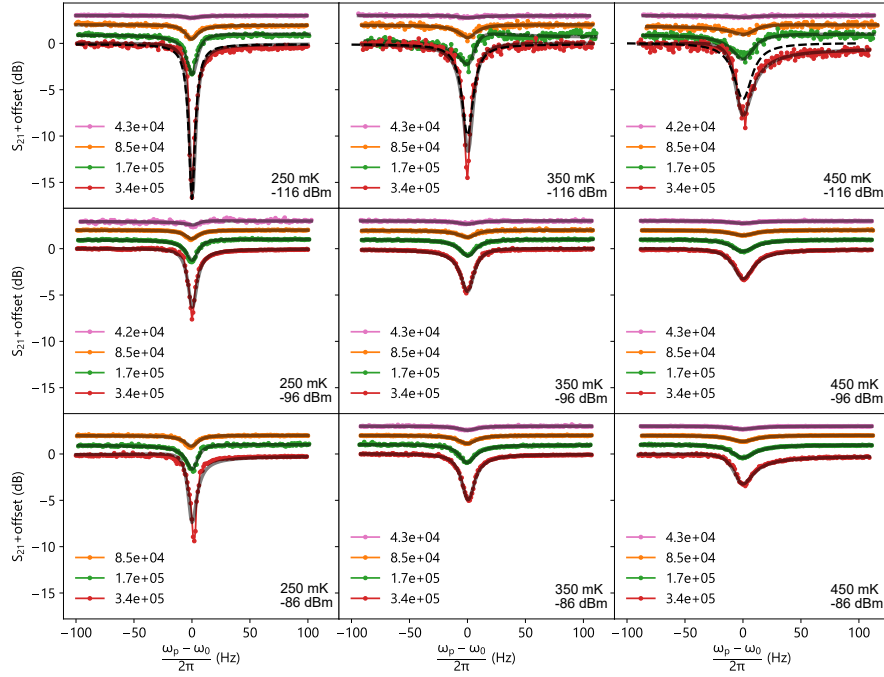


Fig. 4 Probe transmission measurements at the indicated temperatures and probe powers referenced to the input of the cavity. Blue pumping was applied, yielding the specified intracavity pump photon numbers. The transmission curves are offset vertically for clarity and ω_0 is an offset close to ω_c . The curves are fits of Eq. 1 to the data. The dashed black curves show the part of the temperature dependence due to variation of Ω_m and Γ_m (see text).

threshold, we observe a response that is inconsistent with the theory presented here and goes beyond the scope of the present work.

The solid gray curves represent fits of the theoretical $|S_{21}|$ (Eq. 1) to the data, where the values of Ω_m and Γ_m at each temperature are the same as the ones used to fit the red pumping data (Fig. 3). The temperature dependence of Ω_m and Γ_m is not entirely responsible for the temperature dependence of these data: The dashed black curves in the top row of Fig. 4 were generated by retaining the values of Ω_m and Γ_m corresponding to the temperature but setting ω_c and κ to their best fit values at 250 mK and maximum pump power. The dependence of κ on temperature is responsible for much of the discrepancy between the solid gray and dashed black curves but doesn't account for the small asymmetry about the minimum of the solid gray curve. The latter is due to a small detuning from the cavity resonance.

The theoretical transmission is also in excellent agreement with our measurements made further from the microwave resonance. The top row of panels in Fig. 5 shows $|S_{21}|$ as a function of Ω and Δ at the maximum red pumping power ($n_{cav} = 1.3 \times 10^6$) and the specified temperatures and probe powers.

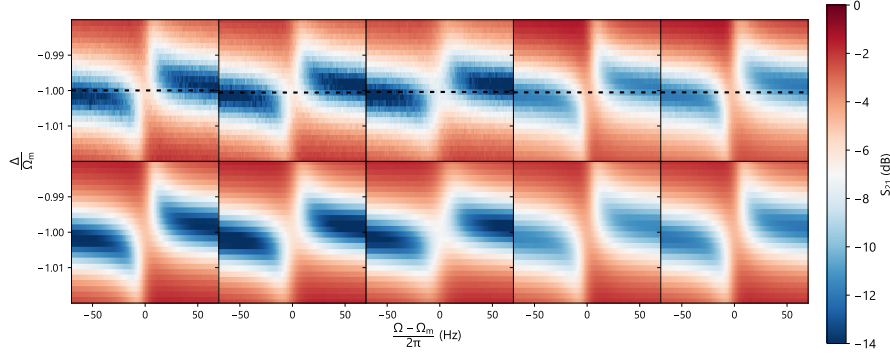


Fig. 5 Measured (upper panel) and theoretical (lower panel) probe transmission at the maximum red pumping power ($n_{cav} = 1.3 \times 10^6$). From left to right the values of [temperature (mK), probe power (dBm), $\kappa/2\pi$ (kHz) and $\Delta\omega_c/2\pi$ (kHz)] are [250, -116, 84, 0], [350, -116, 82, 52], [450, -116, 83, 93], [250, -96, 96, -10], [250, -86, 95, -9], where $\Delta\omega_c$ is the shift in ω_c relative to its value in the leftmost panels. The black dashed lines correspond to data shown in the top row and left column of panels of Fig. 3.

Horizontal line cuts in this figure correspond to particular pump frequencies ω_d and narrow sweeps of ω_p centered on $\omega_d + \Omega_m$. Thus each spectrum appearing as a vertical line in Fig. 2 corresponds to a horizontal line-cut at a particular value of Δ in the upper-left panel of Fig. 5.

In Figs. 2 and 5, the OMIT signal decreases significantly, as expected, when the frequency of the upper mechanical sideband of the pump is not well-aligned with the microwave resonance. In Fig. 2 this condition corresponds to the left and right extremities of the plot and in Fig. 5 it corresponds to the upper and lower extremities of each panel. The fact that the size of the OMIT resonance in Fig. 5 is largest for $|\Delta/\Omega_m + 1| < \approx 0.5\kappa/\Omega_m \approx 10^{-2}$ follows from the condition $|\Delta + \Omega| < \approx \kappa/2$ (Section 2).

The black dashed lines in Fig. 5 are at the optimal pump detuning $\Delta = -\Omega_m$ and correspond to data shown in the top row and left column of panels of Fig. 3. Note that for the pump detuning $\omega_d = \omega_c - \Omega_m$ used in Fig. 3 the quantity on the x-axis of that figure ($\omega_p - \omega_c$) is equivalent to the one on the x-axis of Fig. 5 ($\Omega - \Omega_m$). Thus we have already demonstrated excellent agreement between theory and the data along the black dashed lines in Fig. 5. The panels in the bottom row of Fig. 5 demonstrate the same level of agreement for the case where the upper mechanical sideband of the pump is slightly detuned from the microwave resonance. These panels show $|S_{21}|$ from Eq. 1 with the values of Ω_m and Γ_m corresponding to the temperatures given in the respective upper panels and the indicated best-fit values of κ and ω_c . The increase in κ from 84 kHz to 96 kHz as the probe power is increased from -116 dBm to -96 dBm is comparable to the small fluctuations observed in the dependence of microwave cavity loss on drive power observed in Ref. [28].

The top row of panels in Fig. 6 shows $|S_{21}|$ as a function of Ω and Δ at the maximum blue pumping power ($n_{cav} = 3.4 \times 10^5$) and the specified temper-

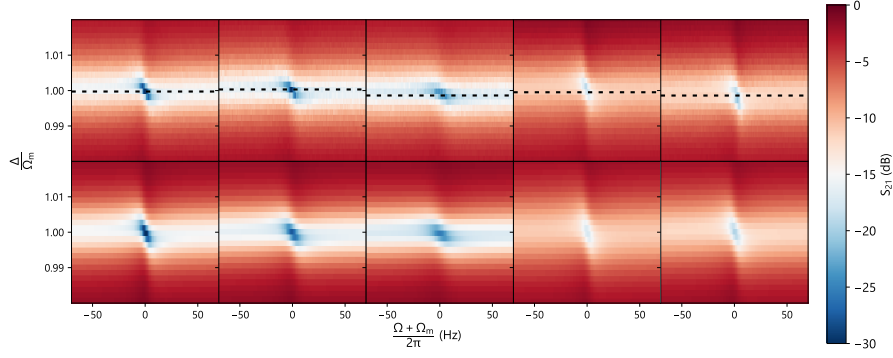


Fig. 6 Measured (upper panel) and theoretical (lower panel) probe transmission at the maximum blue pumping power ($n_{cav} = 3.4 \times 10^5$). From left to right the values of [temperature (mK), probe power (dBm), $\kappa/2\pi$ (kHz) and $\Delta\omega_c/2\pi$ (kHz)] are [250,-116,83,0],[350,-116,80,37],[450,-116,78,80],[250,-96,103,-17],[250,-86,98,-19], where $\Delta\omega_c$ is the shift in ω_c relative to its value in the leftmost panels. The black dashed lines correspond to data shown in the top row and left column of panels of Fig. 4.

atures and probe powers. The panels in the bottom row of Fig. 6 show $|S_{21}|$ from Eq. 1 with the values of Ω_m and Γ_m corresponding to the temperatures given in the respective upper panels and the indicated best-fit values of κ and ω_c . The agreement between theory and experiment is again excellent.

5 Conclusion

Nanomechanical resonators coupled to microwave cavities by radiation pressure constitute ideal systems for microwave amplification and absorption. The amplifiers or filters can have a very low noise level or a very narrow bandwidth, and the gain or attenuation depends very strongly on pump power. Our measurements confirm the applicability of the theoretical transmission Eq. 1 to a larger parameter space than has been covered in previous works. We demonstrated excellent agreement with theory over a wide range of probe frequencies, pump frequencies, probe powers, pump powers and temperatures for both red and blue pumping, thereby facilitating further development of microwave devices based on nanomechanics.

The data used here is available at <https://cloud.neel.cnrs.fr/index.php/s/CnnYPKn8XHYZgXa>.

6 Acknowledgments

This work was supported by the ERC StG grant UNIGLASS No.714692, STaRS-MOC Project No. 181386 from Region Hauts-de-France, ISITE-MOST project No. 201050, and the ERC CoG grant ULT-NEMS No. 647917. The research leading to these results has received funding from the European Union's

Horizon 2020 Research and Innovation Programme, under Grant Agreement no 824109.

References

1. Vion D, Aassime A, Cottet A, Joyez P, Pothier H, Urbina C, Esteve D and Devoret M H 2002 *Science* **296** 886–889
2. Wallraff A, Schuster D I, Blais A, Frunzio L, Huang R S, Majer J, Kumar S, Girvin S M and Schoelkopf R J 2004 *Nature* **431** 162–167
3. Arute F, Arya K, Babbush R, Bacon D, Bardin J C, Barends R, Biswas R, Boixo S, Brandao F G, Buell D A *et al.* 2019 *Nature* **574** 505–510
4. Day P K, LeDuc H G, Mazin B A, Vayonakis A and Zmuidzinas J 2003 *Nature* **425** 817–821
5. Cohadon P F, Heidmann A and Pinard M 1999 *Phys. Rev. Lett.* **83**(16) 3174–3177 URL <https://link.aps.org/doi/10.1103/PhysRevLett.83.3174>
6. Carmon T, Rokhsari H, Yang L, Kippenberg T J and Vahala K J 2005 *Phys. Rev. Lett.* **94**(22) 223902 URL <https://link.aps.org/doi/10.1103/PhysRevLett.94.223902>
7. Kleckner D and Bouwmeester D 2006 *Nature* **444** 75–78
8. Arcizet O, Cohadon P F, Briant T, Pinard M and Heidmann A 2006 *Nature* **444** 71–74
9. Poggio M, Degen C, Mamin H and Rugar D 2007 *Physical Review Letters* **99** 017201
10. Regal C, Teufel J and Lehnert K 2008 *Nature Physics* **4** 555–560
11. O’Connell A D, Hofheinz M, Ansmann M, Bialczak R C, Lenander M, Lucero E, Neeley M, Sank D, Wang H, Weides M *et al.* 2010 *Nature* **464** 697–703
12. Bernier N R, Toth L D, Koottandavida A, Ioannou M A, Malz D, Nunnenkamp A, Feofanov A and Kippenberg T 2017 *Nature communications* **8** 1–8
13. Barzanjeh S, Wulf M, Peruzzo M, Kalaei M, Dieterle P, Painter O and Fink J M 2017 *Nature communications* **8** 1–7
14. Massel F, Heikkilä T, Pirkkalainen J M, Cho S U, Saloniemi H, Hakonen P J and Sillanpää M A 2011 *Nature* **480** 351–354
15. Weis S, Rivière R, Deléglise S, Gavartin E, Arcizet O, Schliesser A and Kippenberg T J 2010 *Science* **330** 1520–1523
16. Safavi-Naeini A H, Alegre T M, Chan J, Eichenfield M, Winger M, Lin Q, Hill J T, Chang D E and Painter O 2011 *Nature* **472** 69–73
17. Teufel J D, Li D, Allman M, Cicak K, Sirois A, Whittaker J and Simmonds R 2011 *Nature* **471** 204–208
18. Hocke F, Zhou X, Schliesser A, Kippenberg T J, Huebl H and Gross R 2012 *New Journal of Physics* **14** 123037
19. Zhou X, Hocke F, Schliesser A, Marx A, Huebl H, Gross R and Kippenberg T J 2013 *Nature Physics* **9** 179–184
20. Ockeloen-Korppi C, Damskägg E, Pirkkalainen J M, Heikkilä T, Massel F and Sillanpää M 2016 *Physical Review X* **6** 041024
21. Bothner D, Yanai S, Iniguez-Rabago A, Yuan M, Blanter Y M and Steele G A 2020 *Nature communications* **11** 1–9
22. Cohen M A, Bothner D, Blanter Y M and Steele G A 2020 *Physical Review Applied* **13** 014028
23. Aspelmeier M, Kippenberg T J and Marquardt F 2014 *Reviews of Modern Physics* **86** 1391
24. Agarwal G S and Huang S 2010 *Physical Review A* **81** 041803
25. Gardiner C and Zoller P 2004 *Quantum noise: a handbook of Markovian and non-Markovian quantum stochastic methods with applications to quantum optics* (Springer Science & Business Media)
26. Clerk A A, Devoret M H, Girvin S M, Marquardt F and Schoelkopf R J 2010 *Reviews of Modern Physics* **82** 1155
27. Zhou X, Cattiaux D, Gazizulin R, Luck A, Maillet O, Crozes T, Motte J F, Bourgeois O, Fefferman A and Collin E 2019 *Physical Review Applied* **12** 044066
28. O’Connell A D, Ansmann M, Bialczak R C, Hofheinz M, Katz N, Lucero E, McKeeney C, Neeley M, Wang H, Weig E M *et al.* 2008 *Applied Physics Letters* **92** 112903